processes

MDPI

Article

The Influence of a Key Indicator k_v on the Diffusion Range of Underwater Oil Spill

Hong Ji [1,2,3,4,*], Yaxin Wang [4,5], Ting Wang [1,2,3], Ke Yang [1,2,3] and Zhixiang Xing [1,2,3]

1 School of Safety Science and Engineering, Changzhou University, Changzhou 213164, China; xingzhixiang@cczu.edu.cn (Z.X.)
2 School of Emergency Management Science and Engineering, Changzhou University, Changzhou 213164, China
3 Institute of Public Safety and Emergency Management, Changzhou University, Changzhou 213164, China
4 Jiangsu Key Laboratory of Oil & Gas Storage and Transportation Technology, Changzhou University, Changzhou 213016, China; 18006126053@163.com
5 School of Petroleum Engineering, Changzhou University, Changzhou 213016, China
* Correspondence: jihong@cczu.edu.cn

Abstract: As oil spills cause harm to the survival and environment of the ocean, the objective of the present paper is to study the oil migration range using the key indicator k_v, which is defined as the ratio of oil spill speed to ocean current speed. The correctness of diffusion models created and estimated for subsea oil spills can be verified by experiments. We also considered the effect of key indicators on the horizontal and vertical dispersion ranges of oil spills. The study's findings show that, under various k_v settings, the horizontal and vertical spreading heights of oil spills both increase as k_v rises. When k_v is equal, the leakage velocity and water flow velocity increase synchronously, and over time, the horizontal distance and vertical diffusion height of the oil spill gradually increase. In the early stages of an oil spill, when k_v = 50, 100, or 150, the vertical spreading velocity will rapidly decrease. The vertical spreading speed of spilled oil increases as k_v rises when the water flow rate remains constant. The horizontal migration distance grows as k_v decreases when the leakage rate is constant. Fitting curves for the vertical rise height and horizontal spreading distance for the same and various k_v settings were also obtained in order to anticipate the migration mode of oil spills. This is critical for dealing with environmental damage caused by maritime oil spills, as well as emergency responses.

Keywords: oil spill; submarine pipeline; physical model experiment; fitting curve; a key indicator k_v

Citation: Ji, H.; Wang, Y.; Wang, T.; Yang, K.; Xing, Z. The Influence of a Key Indicator k_v on the Diffusion Range of Underwater Oil Spill. *Processes* **2023**, *11*, 2332. https://doi.org/10.3390/pr11082332

Academic Editors: Marcin Banach, Olga Długosz and Jolanta Pulit-Prociak

Received: 30 June 2023
Revised: 19 July 2023
Accepted: 25 July 2023
Published: 3 August 2023

1. Introduction

Problems such as the corrosion of submarine pipelines have occurred during the production and transportation of oil and gas, resulting in frequent incidences of underwater oil leaks. Whether it is locations with active oil production around the world or other regions, knowledge of preventing oil leak incidents should be enhanced [1–4]. The bulk of oil spills occur along coasts, sheltered bays, ports, or docks and are close to response resources [5]. Oil spills have a detrimental influence not only on oil safety but also on the survival and habitat of the ocean and related species [6–8]. If the leaked oil accumulates on the sea surface, it will not only affect the operations of nearby vessels but also threaten the safety of the oil platform. Once encountering an open flame, there may be secondary vicious accidents such as fires or explosions. Many large-scale oil spills have occurred worldwide over the past decades, causing tremendous ecological hazards and socioeconomic losses [9,10]. The severity of the damage caused by an oil spill depends largely on the chemical context of the oil, the area affected, and the success of remedial efforts [11,12]. Once an oil spill accident occurs, it is necessary to make an active and rapid response to reduce the harm caused by the spill [13–16]. As a result, it is very necessary to understand the transport state of oil

droplets under water. Furthermore, laying oil containment booms, as a basic way to control oil dispersal, also depends on the rising speed of oil spread and the trend of spreading. Therefore, an exact prediction of the oil spill process and dispersal could provide useful information for setting up an oil containment boom and reducing the damage of future oil spills [17].

With the gradual expansion of underwater oil exploitation and the gradual increase in underwater oil and gas transportation [18], studying the diffusion and drift processes of underwater oil spills is of great significance for relevant departments to take emergency measures and reduce the risk of accidents and the pollution [19–21]. In recent years, there have been many oil spill accidents caused by large-scale blowouts, and many scholars have conducted research on them [22,23]. Haibo Chen [24] has established a numerical model for oil spills from blowouts that simulates the underwater transportation and fate of oil spills in deep water. It is specifically used to simulate hypothetical oil spill events that occur on the seabed of deep-water oil and gas fields in the South China Sea. P. M. Paiva's [25] research findings emphasized the importance of three-dimensional methods for oil spill scenarios in deep and ultradeep water wells, especially when considering the injection of dispersants into the leak source. Scholars from China and other countries have performed extensive research on the elements that influence the spread of underwater oil spills [26–28]. One of them, Yuan Sun [29], used simulation to determine the impact of underwater oil spill density on the time it took for the oil to reach the sea surface. Using the two-dimensional numerical simulation VOF model, Cao Xuewen [30] discovered that, in the presence of a wave ocean current, the time it takes for the oil to rise to the water's surface grows as its density rises and that its height essentially varies linearly over time. The corresponding time for oil leakage to reach the same horizontal distance increases as oil density increases; Chen Jiayue [31] measures the scope of oil spill diffusion using the measuring parameter Fr0 (density Froude constant). The driving force of a floating jet involves both momentum and buoyancy, and the ratio of inertia force to buoyancy force, represented by momentum, is critical to the jet movement. Additionally, the oil spill's diffusion range is impacted by the jet velocity near the leakage site. According to Cosan Daskiran, the thickness of the shear layer at the orifice is the primary factor influencing the size of droplets that separate from liquid jets. The size of the droplet increases with the thickness of the shear layer at the nozzle. The increase in shear layer thickness and instability in the jet direction cause the droplet size to grow [32]; To simulate how oil and gas will behave in deep-sea well explosions, Yapa has created a 3D model. The model incorporates jet/plume fluid mechanics, jet/plume thermodynamics, and the dynamics and thermodynamics of hydrate formation [33]. According to a formula developed by Fanghui Chen, a multiphase jet/plume model, the effect of gas separation from the primary plume under cross-flow conditions is explained [34]. Mohammadmehdi Raznahan [21] explored the behavior of oil in nearshore locations at various wave and current velocities and developed a three-dimensional numerical model of transient three-phase flow. Johansen and Yapa [35] performed an experimental investigation on the oil droplet size of the spilled oil and discovered that the size of the oil droplet impacts the spilled oil. To explore the distribution properties of oil droplet size before and after adding oil dispersant and varying flow rates, oil and gas ratios, and the influence of the diffusion range, a cylindrical pool with a diameter of 3 m and a height of 6 m was built in the SINTEF laboratory [36]. The distribution of oil droplets and bubble particle size, according to Qi Junliang [37] and other studies [38], impacts the rate of hydrate growth, the rate of dissolution, and the position and timing of the oil and gas rising to the surface; Zang Xiaogang's [39] simulated research looked at how the oil spill aperture affected the oil's underwater drift and diffusion. Yang Yi [40] investigated the impact of varied leakage angles on the drift trajectory of oil spill dispersion. Through tests and simulations, Xiang Ziyang [38] investigated the effects of temperature and the position of the oil pipeline in the deep sea on the horizontal migration distance and time of the oil leak. Research on the relationship between oil spill and seawater speed has been carried out (seawater speed involves wave height, wavelength, etc.) by

Chen Jiayue [31] and Gao Qingjun [41]. Gao Qingjun [41] studied the influence of wind speed on the scope of oil spill by simulating underwater oil spill. Hong Ji [42] used tests and numerical simulations to simulate the impacts of different oil leakage rates and different ocean current speeds on the underwater oil spill, and then fitted the linear fitting curve.

The migration trajectory of the leaked oil is affected by each of the components in the aforementioned studies to a different extent. However, the majority of them are single-factor studies that do not account for the complexity of the factors impacting an undersea oil spill. The diffusion range of an underwater oil spill is comprehensively affected by ocean current speed and oil spill speed. This paper primarily considers the influence of oil spill speed and water flow speed on the spread of an oil spill and an indicator k_v (the ratio of oil spill speed to ocean current speed); speed is a scalar quantity that only considers size and does not involve directional issues. k_v is the ratio of speeds and was defined, and the law of oil spill diffusion under different k_v was studied, which provided an effective reference for guiding the treatment of underwater oil leakage accidents and marine environmental pollution.

2. Simulation Method

In this paper, a two-dimensional numerical simulation of an underwater oil spill was adopted, and the VOF multiphase flow method was selected to track the migration process of an underwater oil spill. The VOF model is a numerical model used to simulate multiphase flow in fluid mechanics simulation. It is widely used to study the interaction and interface behavior between different phases such as liquid and gas, and liquid and solid. The VOF model is based on the concept of a volume fraction, dividing the fluid domain into regions of different phases. The volume occupied by each phase in the fluid domain is represented by the corresponding volume fraction, which represents the proportion to the total volume. The VOF model equation [43,44] is:

$$\rho = \alpha\rho + (1-\alpha)\rho \tag{1}$$

$$\mu = \alpha\mu_{water} + (1-\alpha)\mu_{oil} \tag{2}$$

$$\frac{\partial(\rho u)}{\partial t} + \nabla\cdot(\alpha u) = 0 \tag{3}$$

$$\frac{\partial\left(\rho\vec{u}\right)}{\partial t} + \nabla\cdot\left(\rho\vec{u}\vec{u}\right) = -\nabla\cdot p + \nabla\cdot\vec{\tau} + \rho\vec{g} + \vec{f} \tag{4}$$

where p is the pressure, $\vec{g}$ is the acceleration due to gravity, $\vec{\tau}$ is the stress tensor, and $\vec{f}$ describes the forces interacting with phases such as surface tension.

The diffusion processes of underwater oil spills all follow the three laws of conservation of mass, conservation of momentum, and conservation of energy. The RANS equation is used to describe the fluid flow, including the following mass conservation equation and momentum conservation equation [21,45]:

$$\frac{\partial\rho}{\partial t} + \frac{\partial}{\partial x_i}(\rho u_i) = 0 \tag{5}$$

$$\frac{\partial u_i}{\partial t} + \frac{\partial u_i u_j}{\partial x_j} = -\frac{\partial\overline{p}}{\rho\partial x_i} + v\nabla^2 u_i - \frac{\partial x_i' x_j'}{\partial x_j} + g_i \tag{6}$$

Among them, u_i and u_j represent the instantaneous speed components in the i and j directions, respectively, and x_i represents the spatial coordinates in the i direction; g_i is the gravitational acceleration in the i direction; t represents time; p represents pressure; ρ and v represent density and kinematic viscosity.

The realizable k-ε turbulence model includes two equations of turbulent kinetic energy and turbulent energy dissipation rate, as follows [45–48]:

$$\rho\frac{\partial k}{\partial t}+\rho u_i\frac{\partial k}{\partial x_i}=\frac{\partial}{\partial x_i}\left[\left(\mu+\frac{\mu_t}{\sigma_k}\right)\frac{\partial k}{\partial x_j}\right]+G_k+G_b-\rho\varepsilon \tag{7}$$

$$\rho\frac{\partial \varepsilon}{\partial t}+\rho u_i\frac{\partial \varepsilon}{\partial x_i}=\frac{\partial}{\partial x_j}\left[\left(\mu+\frac{\mu_t}{\sigma_\varepsilon}\right)\frac{\partial \varepsilon}{\partial x_j}\right]+\rho C_1 S\varepsilon-\rho \tag{8}$$

Among them:

$$\mu_t=\rho C_\mu\frac{k^2}{\varepsilon}\quad G_k=-\rho\overline{u_i}'\overline{u_j}'\frac{\partial u_j}{\partial x_j}\quad G_b=-g\frac{\mu_t}{\mathrm{Pr}_t}\frac{\partial \rho}{\rho\partial x_i}$$

$$C_1=\max\left(0.43,\frac{\eta}{\eta+5}\right)\quad \eta=S\frac{k}{\varepsilon}\quad S=\sqrt{2S_{ij}\cdot S_{ij}}$$

$$S_{ij}=\frac{1}{2}\left(\frac{\partial u_i}{\partial x_j}+\frac{\partial u_j}{\partial x_i}\right),\ C_1=1.44,\ C_2=1.92,\ C_\varepsilon=1,\ C_\mu=0.09,\ \mathrm{Pr}_t=0.85,\ \sigma_k=1,\ \sigma_\varepsilon=1.2$$

In these equations, G_k and G_b represent the average speed gradient and turbulent energy k caused by buoyancy, respectively; k and ε represent the enthalpy per unit mass and the turbulent energy dissipation rate, respectively; σ_k and σ_ε are turbulent Prandtl numbers; μ and μ_t denotes dynamic viscosity and turbulent viscosity, respectively. The VOF method is a solution to the fluid volume fraction equation based on the mixed phase momentum equation. In the process of underwater oil leakage, F_w and F_o represent the fluid volume fraction in the water phase area and the oil phase area, respectively. The physical meaning of the F function is the fraction of the liquid phase volume of a unit. The liquid volume functions F_w and F_o are written as follows [49,50]:

$$F_w=\frac{V_w}{V_c} \tag{9}$$

$$F_o=\frac{V_o}{V_c} \tag{10}$$

Among them, F_w and F_o are volume functions of water and oil, respectively; V_c, V_w, and V_o are the unit volume and volume of water and oil, respectively, and subscripts w and o represent water and oil, respectively. The two-dimensional transport equation's fractional function is as follows:

$$\frac{\partial F_w}{\partial t}+\frac{\partial uF_w}{\partial x}+\frac{\partial vF_w}{\partial y}=0 \tag{11}$$

$$\frac{\partial F_o}{\partial t}+\frac{\partial uF_o}{\partial x}+\frac{\partial vF_o}{\partial y}=0 \tag{12}$$

The density and kinematic viscosity are as follows:

$$\rho=(1-F_O)\rho_w+F_o+\rho_o \tag{13}$$

$$\nu=(1-F_O)\nu_w+F_o\nu_o \tag{14}$$

3. Underwater Oil Leakage Experiment

The experiment on a maritime oil leak will have an impact on the ecosystem, and the oil used in the experiment is challenging to recover. The actual undersea oil pipeline leak experiment is also rather pricey. As a result, China and the vast majority of nations forbid

experimentation with oil spills at sea. This study uses a water tank to simulate saltwater for studies on underwater oil spills [51].

3.1. Experiment Preparation

The experiment was performed in a tank of water. The rectangular, parallelepiped shape of the lab-specific water tank measures 2.4 m by 1.2 m by 0.6 m (length, width, and height). The clear plexiglass water tank has an 18-mm glass wall thickness.

(1) Oil for experimentation. The oil used in the oil leakage experiment had a density of 0.915 g/mL and a viscosity of 56 mPa·s [42].
(2) An oil well pump. The pump utilized in the experiment has a rated power of 880 W, a speed of 10,000–25,000 r/min, a minimum flow rate of 30 L/min, and a maximum flow rate of 100 L/min.
(3) A high-speed camera.
(4) Other experimental tools and materials. The oil spill pipe is a PVC pipe with an inner diameter of 30 mm and a wall thickness of 1.5 mm; the oil hose has an inner diameter of 33 mm and an outer diameter of 40 mm; and the total capacity of the oil drum is 45 L.

3.2. Experimental Method

Before flowing through the valve and the oil barrel, the oil spill pipeline is connected to the oil pump via the water tank. During the experiment, we adjusted the different oil pump gears to determine the different leakage speeds of the oil product, turned on the oil pump, opened the leakage valve after the oil product started to flow at a constant speed, and used a high-speed camera to record the oil spill process, as shown in Figures 1 and 2.

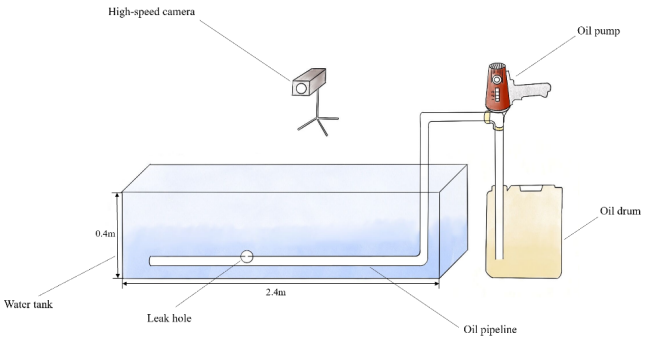

Figure 1. Diagram of experimental equipment.

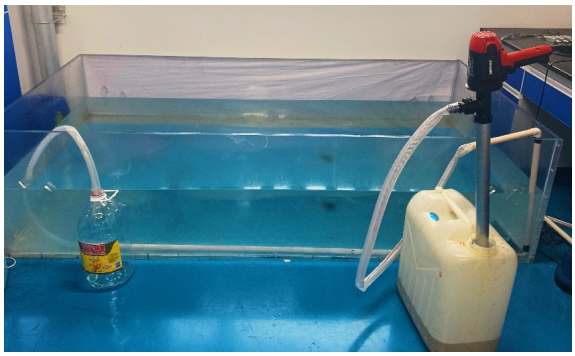

Figure 2. Oil spill experiment facility.

3.3. Comparative Analysis of Experimental and Simulation Results

It is vital to compare the experimental results with the simulation results in order to ensure the model is trustworthy. The simulation's surroundings and discharge situation are identical to those in the experiment. The rectangular area that a high-speed camera

caught during the experiment is referred to as the leakage range. The water depth in the experiment is 0.4 m, the leakage range's total length is 2.4 m, and the water flow rate is 0 m/s. The oil pump's flow rate at various gear ratios was used to approximate the experiment's leakage pace. There are six gears in all, with the third gear having a 58 L per minute pumping capability. With a 3 mm leaking hole diameter, the computed leakage speed is 1.9693 m/s. The experiment's fixed parameters are the leakage aperture and leakage velocity. The three-dimensional physical model is reduced to two dimensions. The leakage diameter is set to be the equivalent diameter of the circular hole, and the overflow diameter is set at 3 mm. We set the simulation calculation area to 0.4 × 2.4 m and placed the leakage port in the middle of the pipeline, 1.2 m away from the right water tank wall. Figure 3 shows the simulated and experimental oil leak patterns for 2.6 s and 3.4 s. The simulated and experimental oil spills have a similar general shape. In the experiment, we placed a scale exactly above the leakage point to measure the height of the oil spill at different times and compare the findings of the experiment and simulation. The comparative results are shown in Figure 4, and the general trends of the simulated and experimental data are essentially the same.

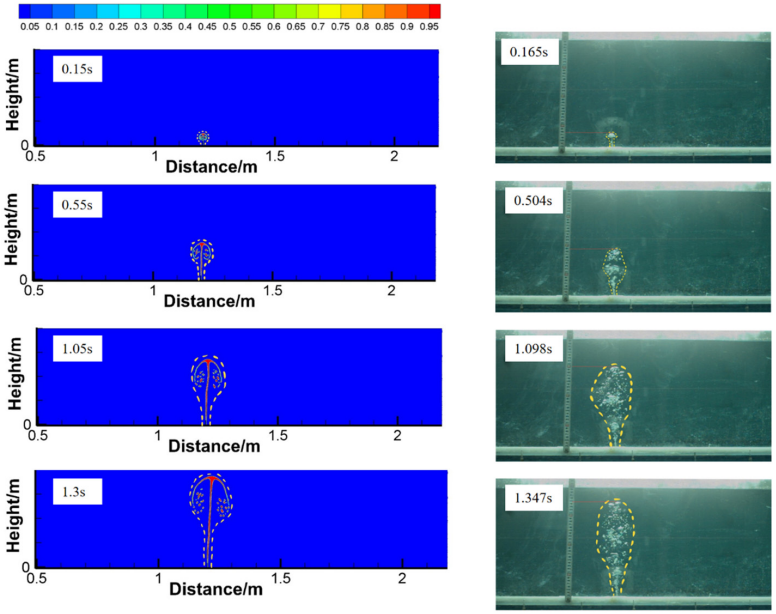

Figure 3. Comparison of underwater oil spill simulation and experimental results.

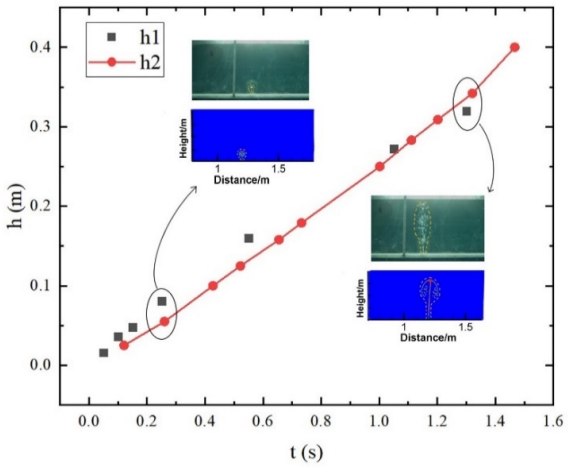

Figure 4. Comparison of the experimental and simulated values of the vertical migration distance. (h1: Experimental values; h2: Simulation values).

Experiment and simulation findings almost always have differences, and the differences can never be zero. The experiment was conducted indoors, and the model was set to normal atmospheric pressure, thus there may have been some differences. Pressure magnitude may have an effect on the diffusion of underwater pipeline leaks, such as the effects on the vertical climbing height. Furthermore, there may be some differences in temperature measurement equipment in the experimental setting and the actual temperature. The water temperature measured at different times, as well as the seawater temperature in the ocean, differ, and the temperature has an effect on the spreading condition. Comparatively speaking, the difference in error between the experiment and the numerical simulation is extremely minor and falls within acceptable bounds.

4. Simulation Method

The two-dimensional single-hole undersea oil spill calculation domain is 40 m × 30 m (X × Y). Because of the overall simplicity of the computational model in this article, a structured grid is chosen and the area around the leaking hole is encrypted to ensure optimal time and storage space. Figure 5 depicts the grid division outcomes. There are 97,955 grids in the two-dimensional underwater single-hole oil spill model. The grid quality of the two-dimensional single-hole undersea oil spill model is 0.89–1 after testing in software, which passes the standards.

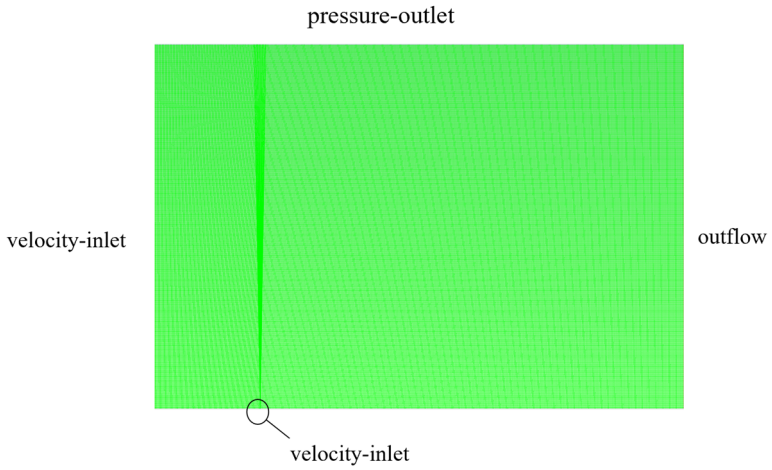

Figure 5. Two-dimensional underwater single-hole oil spill model.

The mesh size of the oil leaking component in this study is small, and the single precision solver is difficult to solve, hence the double precision solver is used for this model. When oil flows from the sea, the velocity and shape of the oil droplets change frequently. Transient calculations are used to simulate and monitor changes in oil spills at any given time. The PISO algorithm is an implicit operator segmentation approach based on the pressure that is commonly used for proximity correction. The PISO algorithm is better suitable for transient calculations than other algorithms, and a corrective step is inserted during the iteration process to make the iteration converge faster.

The time step is set to 0.01 s, with a total of 1000 iterations to capture changes in oil spill spreading within 10 s.

Figure 6 is a schematic illustration of the scope and boundary conditions of the undersea oil spill calculation region. The calculating area is a two-dimensional rectangle with a length of 40 m and a height of 30 m. The calculation area is full of water and the water flows from left to right. We set the leakage hole at 0.05 m, 8 m away from the water inlet.

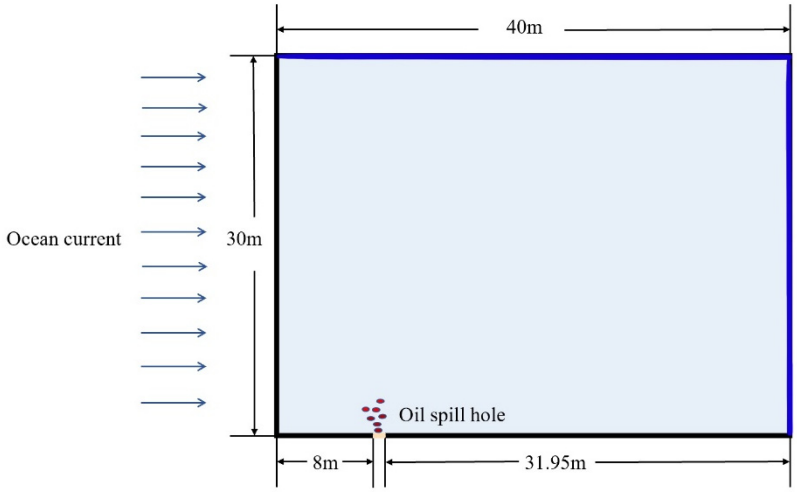

Figure 6. Schematic diagram of the calculation area for the diffusion and drift of crude oil leakage in the ocean current wave environment.

The calculating area's water depth is shallow, and the stratification of seawater density is not taken into account. The density of seawater is set at 998.2 kg/m^3, the density of crude oil is set at 830 kg/m^3, and the viscosities of seawater and petroleum are set at 1×10^{-3} and 5×10^{-2} Pa·s, respectively.

In the coupling method of unsteady speed and pressure, the PISO algorithm is adopted [52,53], and the implicit volumetric force option is enabled to partially balance the pressure gradient and volumetric force of the momentum equation, so as to improve the stability of the oil diffusion and drift model in the gravitational field, and to carry out coupling calculations between the leakage port and the environmental flow field.

This paper considers the influence of different ocean current speeds and water current speed ratios on leakage oil diffusion and drift behavior. Table 1 lists the corresponding calculation conditions (k_v = leakage speed/ocean current speed).

Table 1. Pipeline leakage speed, water flow speed, and k_v under different working conditions.

Water Speed / Leakage Rate	0.2 m/s	0.4 m/s	0.6 m/s	0.8 m/s	1.0 m/s	k_v
Case 1~5	10 m/s	20 m/s	30 m/s	40 m/s	50 m/s	50
Case 6~10	20 m/s	40 m/s	60 m/s	80 m/s	100 m/s	100
Case 11~15	30 m/s	60 m/s	90 m/s	120 m/s	150 m/s	150
Case 16~20	40 m/s	80 m/s	120 m/s	160 m/s	200 m/s	200
Case 21~25	50 m/s	100 m/s	150 m/s	200 m/s	250 m/s	250

5. Numerical Results and Discussion

5.1. The Impact of Ocean Currents on the Spread of Oil Spills

Different ocean current speeds' working environments are compared. Figure 7 depicts the 7 s process of oil spreading from the leak to the water's surface under various working conditions (case 16: Ocean current speed is 0.2 m/s; case 26: Ocean current speed is 0.4 m/s; case 27: Ocean current speed is 0.8 m/s; the leakage speed of three working conditions is 40 m/s).

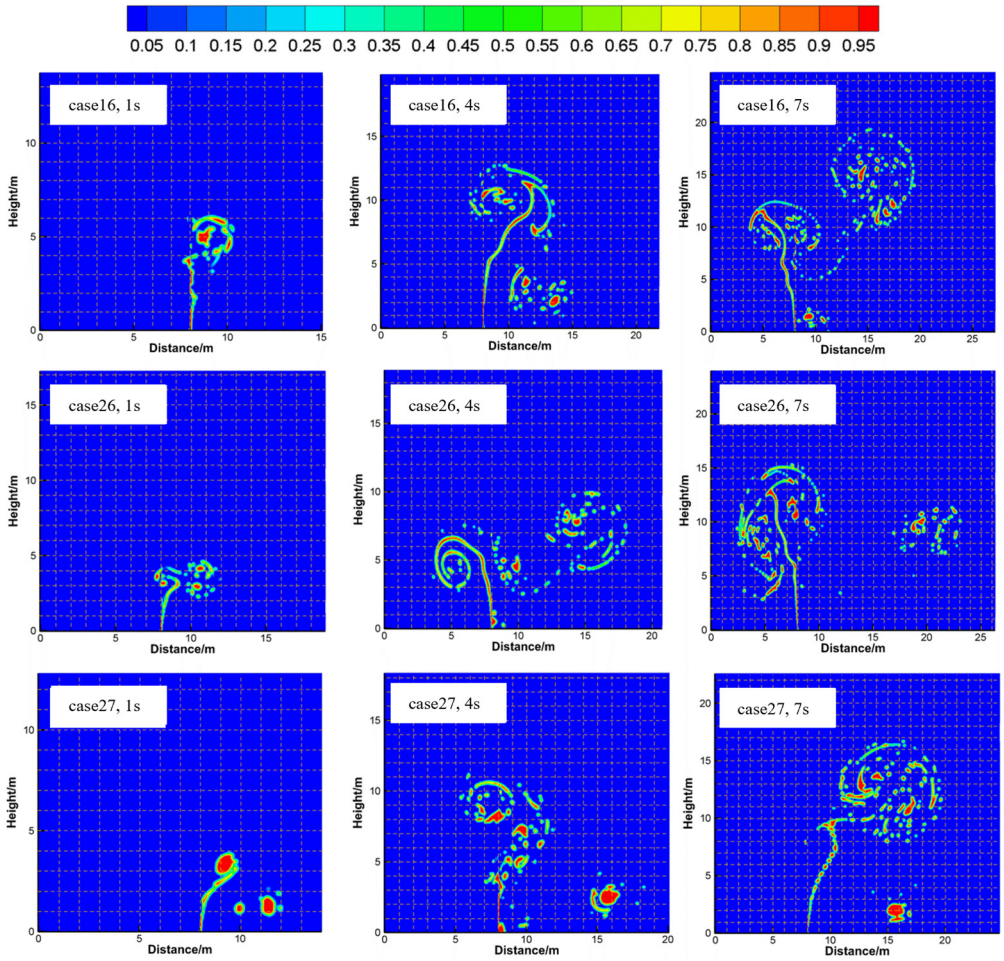

Figure 7. The migration patterns of underwater oil spills at different ocean current speeds.

Under the three working conditions, the maximum height of the oil leak can reach 19.53 m, 15.51 m, and 16.88 m in 7 s, respectively. The simulation figure at 1 s shows that there will be a process of vertical rise at the start of the oil spill and leaking. This is due to the fact that at the start of an oil leak, the leakage speed is dominating, causing the leakage to produce a vertical columnar oil flow. The oil column tilts to the right as the oil droplets reach a specific height, displaying a huge number of dispersed oil droplets. The height of the initial rise in oil for the ocean environment is almost the same due to the influence of inertia force on the leak mouth crude oil being greater than that of shear force, gravity, buoyancy, and inertia force. The current shear effect started to appear as the height of the oil spill rose progressively. With time, the slope of the corresponding spreading height curve declines and the oil droplets diffuse downstream as a group, taking longer to reach the water's surface. Additionally, the leaking oil starts to tilt downward and gradually diffuses downward. The oil spill, which has an ocean current speed of 0.8 m/s, accumulates downward on the sea floor, as seen in the simulation figure at 7 s.

Figures 8 and 9 show, respectively, how oil products drift when subjected to the influence of the action of different ocean currents. When the ocean current speed increases, the rising height of oil spills will gradually decrease, and the rate of rising height will not remain unchanged all the time. The rate will decrease over a period of time. The horizontal drift distance of the oil spill shows an increasing trend, and the increase in the ocean current speed will make the pollution range of the oil spill larger.

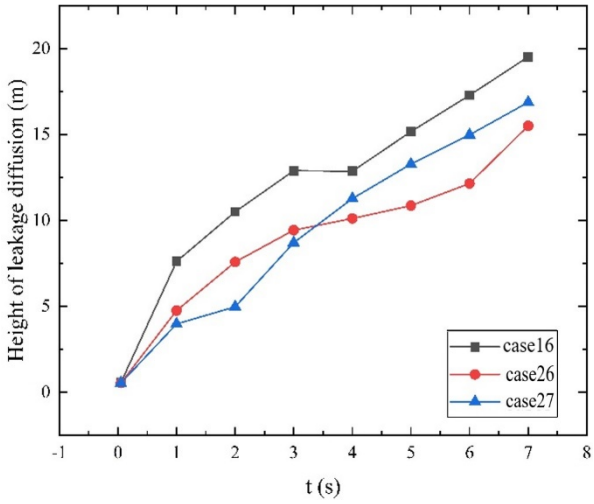

Figure 8. Changes in oil spill rising height under different ocean current speeds.

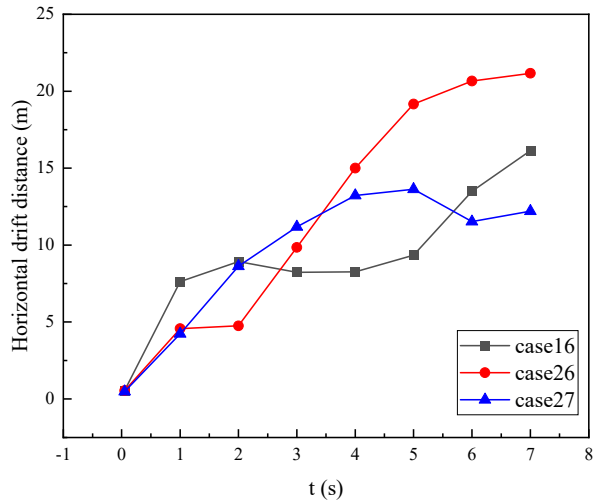

Figure 9. Changes in oil spill horizontal migration distance under different ocean current speeds.

5.2. The Impact of Oil Spill Rate on Oil Spill Spread

When comparing the oil spill patterns of different leakage speeds (case 1: Leakage speed 10 m/s; case 11: Leakage speed 30 m/s; case 21: Leakage speed 50 m/s; three working conditions ocean current speed are all 0.2 m/s), Figure 10 illustrates the change in the spread of the oil spill within 7 s. When the leaking time is 1 s, the height of the vertically ascending oil column progressively grows as the leakage speed increases. This is because the first oil spill speed prevails, and the initial kinetic energy causes the oil to climb vertically. As the length of the oil leak expands, the oil spill is impacted by ocean currents and begins to tilt to the right. At 7 s, the number of oil droplets spread by the oil leak grew, as did the area of oil spill pollution, the oil spill speed, and the oil droplet spreading range. Figure 11 is the curve of the rising height of oil at different leakage speeds with time. The maximum heights reached by the oil spilled within 7 s are 5.99 m, 15.68 m, and 20.92 m, respectively. Under the conditions of the same ocean currents, the rising height of the leaked oil varies with the leakage speed. As the leakage speed increases, the slope of the curve also increases. When the leaking speed is constant, the slope of the spread height curve tends to go down as the rising height rises gradually, especially when the oil spill spreads to the water's surface. Figure 12 shows the variation of the horizontal spreading distance of crude oil with different leakage rates over time. It can be seen from Figure 12 that the greater the leakage speed, the faster the spread of spilled oil when it reaches the water surface, the wider the range of spreading levels, and the more serious the pollution

to the marine environment. When the spilled oil spreads over a certain period of time, the horizontal spreading speed will decrease.

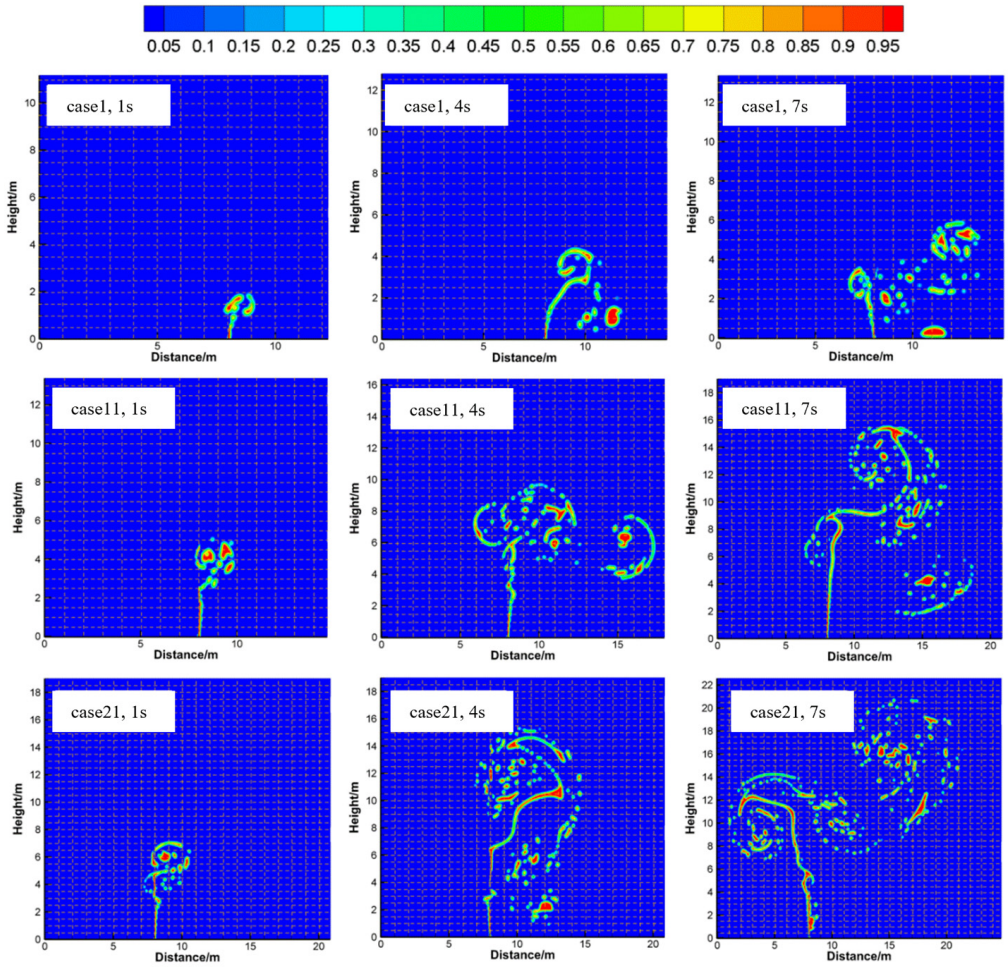

Figure 10. The migration patterns of underwater oil spills at different leakage rates.

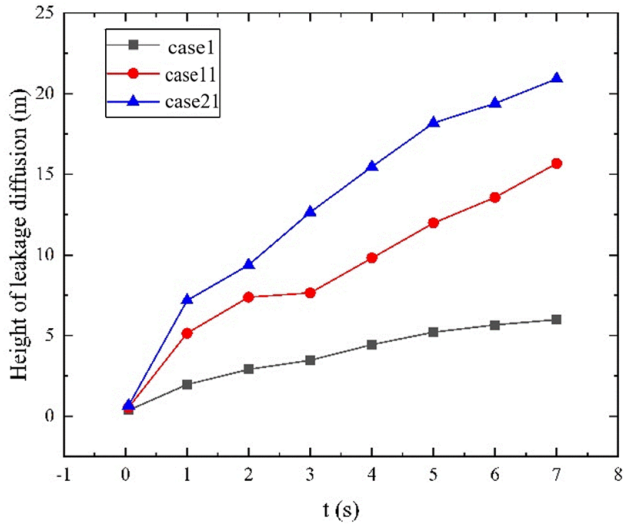

Figure 11. Changes in oil spill rising height under different leakage rates.

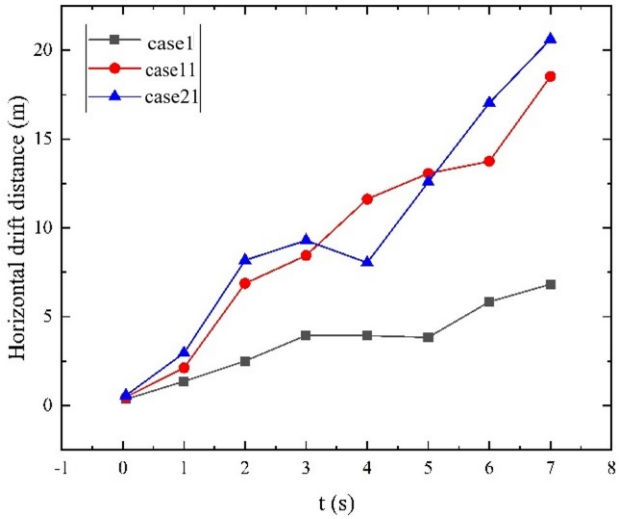

Figure 12. Changes in oil spill horizontal migration distance under different leakage rates.

5.3. The Influence of Different k_v on the Spread of Oil Spill

Numerical simulations were run under settings in which the leakage velocity to ocean current velocity k_v ratio was 50, 100, 150, 200, and 250, respectively. Table 2 shows the matching leakage velocity and ocean current velocity for various k_v. Figures 13 and 14 depicts a cloud diagram showing oil spill diffusion and migration.

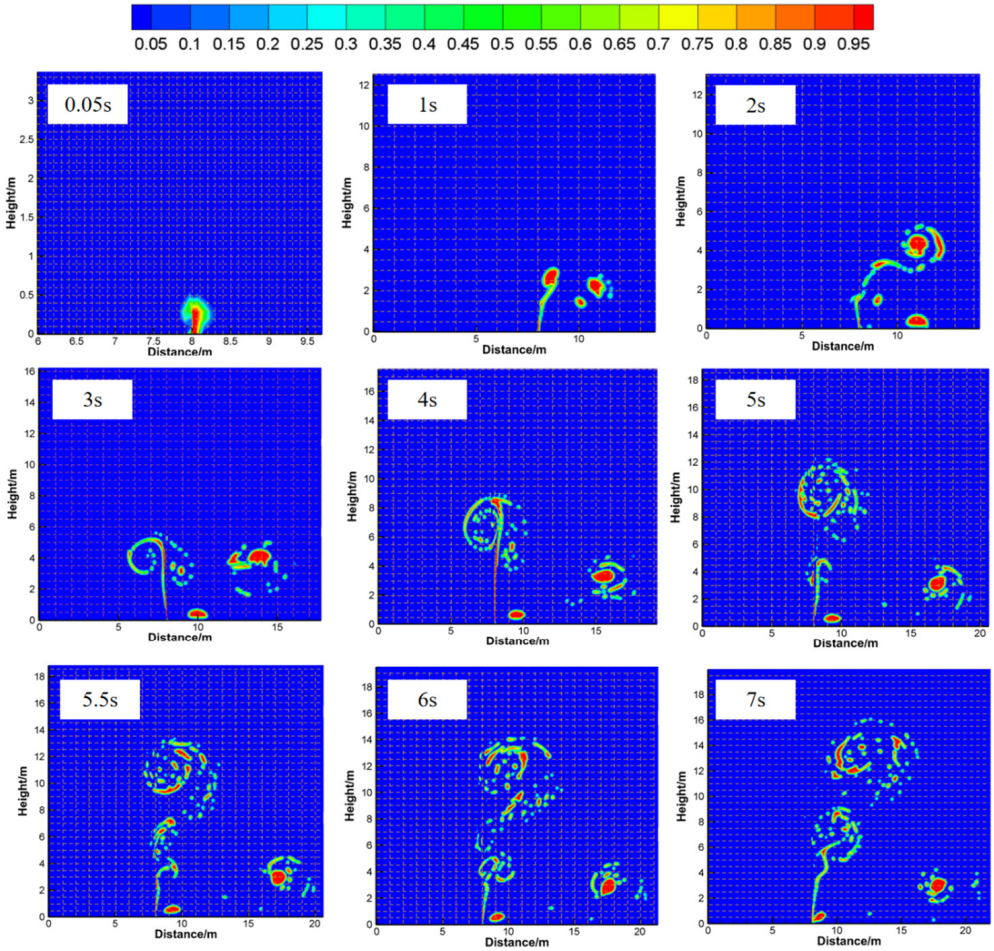

Figure 13. Ocean current velocity of 0.6 m/s, leakage speed of 30 m/s, k_v = 50, oil spill spreading.

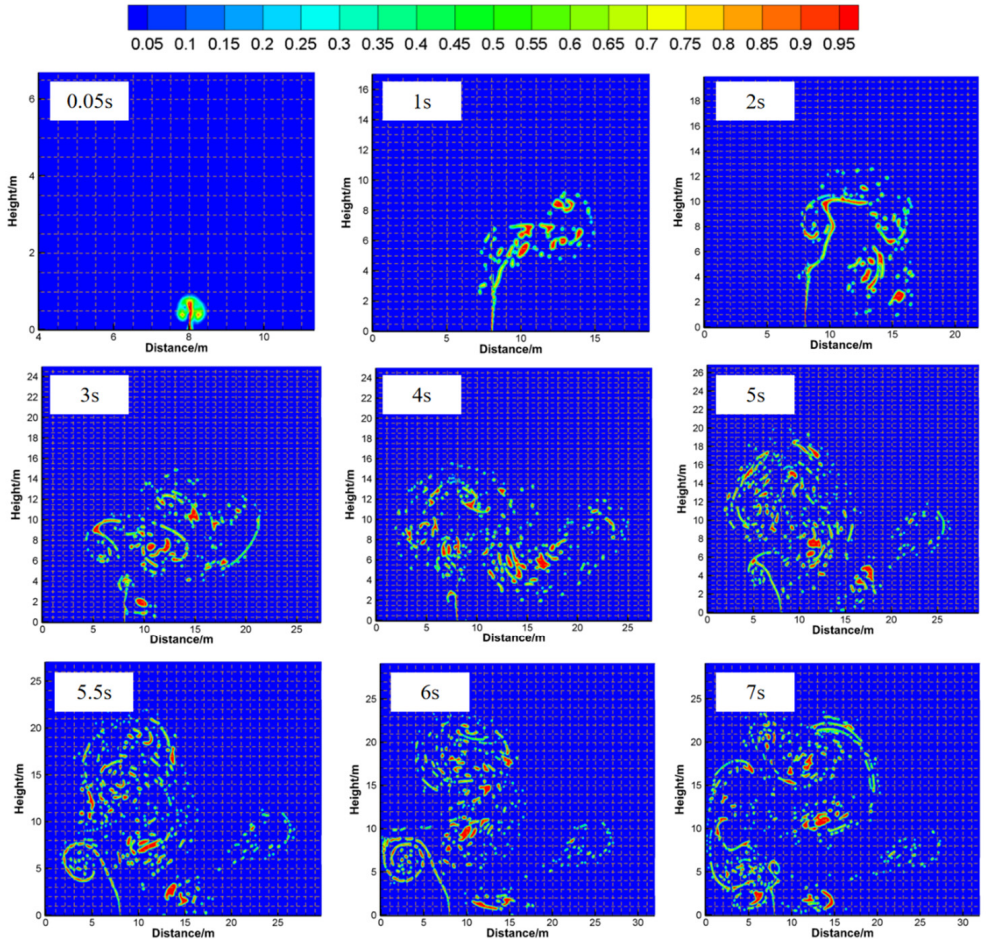

Figure 14. Ocean current velocity of 0.8 m/s, leakage speed of 200 m/s, k_v = 250, oil spill spreading.

Table 2. Corresponding leakage velocity and ocean current velocity values at different k_v.

Water Speed / Leakage Rate	0.6	0.8 m/s	0.8 m/s	1 m/s	0.8 m/s
k_v	30 m/s 50	80 m/s 100	120 m/s 150	200 m/s 200	200 m/s 250

Analysis of multiple oil spill velocities based on the same water flow velocity. The faster the oil flow, the greater the vertical spreading height, and the less oil spill accumulates on the right side. When the leakage speed is the same and the current speed is different, the higher the current speed, the more oil spills accumulate on the right side. That is, when the water flow velocity remains constant as k_v increases, so does the vertical spreading velocity of the oil spill. As shown in Figure 15, When the leakage rate is constant, as k_v lowers, the horizontal spreading distance increases. It can be seen that the accumulation of oil spills to the right is controlled by the combined effect of oil spill speed and ocean current speed. The spreading range increases with the increase in leakage intensity, and the greater the degree of leakage, the larger the spreading range. The petroleum product with k_v = 50 diffuses in the form of an oil column for 1 s during an oil spill. Within one second, the oil with k_v = 250 generated dispersed oil droplets. After a 7-s oil release, oil spreading with k_v = 250 virtually fills the entire simulated region. As seen in Figure 16, the leakage Vertical diffusion height corresponding to kv = 250 tends to stabilise as time passes.

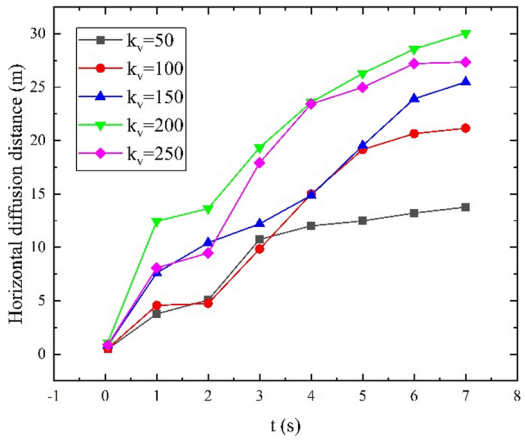

Figure 15. The horizontal distance of underwater oil spill spreading with different k_V.

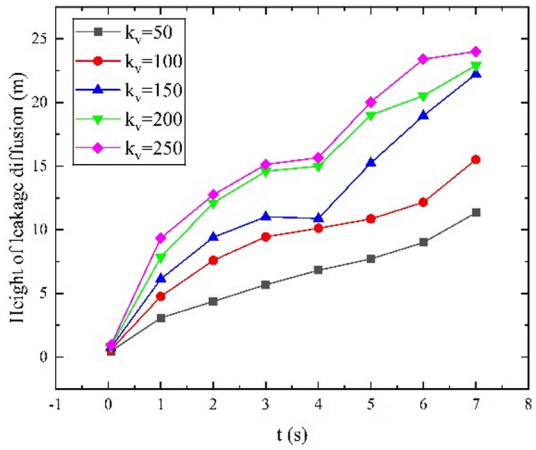

Figure 16. The height of underwater oil spill spreading with different k_V.

Figure 17 shows the trend of the horizontal average speed of oil spill diffusion. It can be seen that after 6 s, the slope of the line graph of the average migration speed of oil products tends to be the same, that is, the actual acceleration of oil product horizontal spreading is almost the same. When the time is long enough, the change in k_V has little effect on the acceleration of oil spill diffusion.

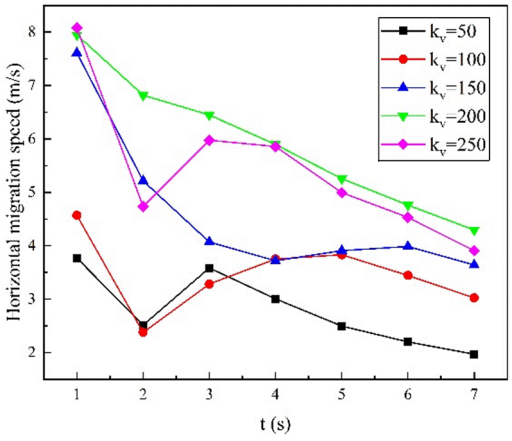

Figure 17. Horizontal migration speed of underwater oil spills with different k_V.

As shown in Figure 18, with an increase in k_V, the vertical spreading speed of spilled oil gradually increases, but when k_V is the same, the vertical migration speed gradually

decreases with the increase in time. When the migration time exceeds 2 s, the vertical migration speed curves corresponding to different k_v have nearly the same trend and almost the same slope, and the acceleration of oil vertical migration is also nearly the same. When k_v = 50 and k_v = 100, the vertical spreading speed of the oil spill has been in a steady downward trend within 6 s, and there is an increasing trend after 6 s; when k_v = 150, k_v = 200, and k_v = 250, the vertical spreading speed of the oil spill decreased greatly in 1–2 s, and the vertical speed of 2–3 s increased to a certain extent, and the speed of 3–4 s began to decline, and then increased for a period of time after the decline. Different k_v values correspond to the oil spill at 6–7 s, and after that, the time speed change gradient is relatively similar, achieving a relatively stable condition. The bigger the k_v, the greater the reduction in vertical spreading speed of the oil spill in 1–2 s; the smaller the k_v, the slowest the vertical speed change.

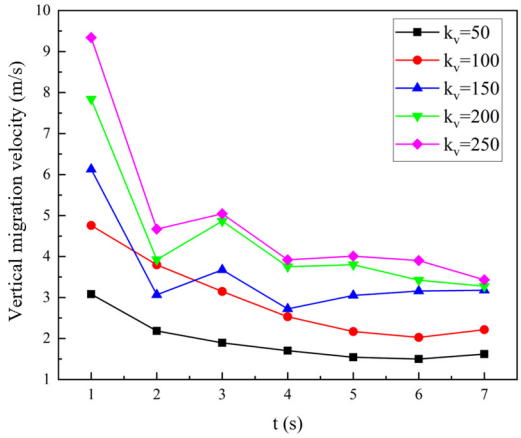

Figure 18. Vertical spreading speed of underwater oil spills with different k_v.

The maximum height that can be attained when oil spills of 7 s of varying k_v are simulated to generate Figure 19, adjustment coefficient R^2, and fitting curve formula is as follows:

$$y = 3.274 + 0.17x - 3.491x^2 \quad (15)$$

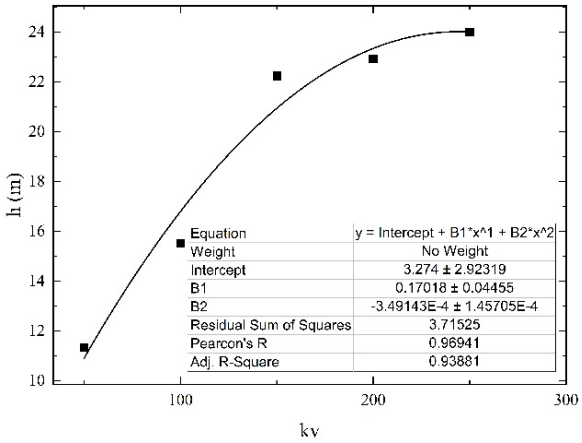

Figure 19. Fitting curve of the maximum height h that an oil spill can reach at various k_v within 7 s.

With the increase in k_v, the maximum height of oil spill spreading keeps rising, but the extent of the rise gradually decreases, and the rising curve gradually flattens out.

Figure 20 shows the furthest distance of horizontal migration of an oil spill within 7 s under different k_v. With the gradual increase in k_v, the furthest distance of horizontal spreading of an oil spill does not always increase. When k_v =200, the furthest distance

of horizontal spreading of an oil spill is 30.06 m. The simulated data were fitted, and the adjustment coefficient R^2 was 0.979. The fitting formula was as follows:

$$y = 2.776 + 0.243x - 5.697x^2 \quad (16)$$

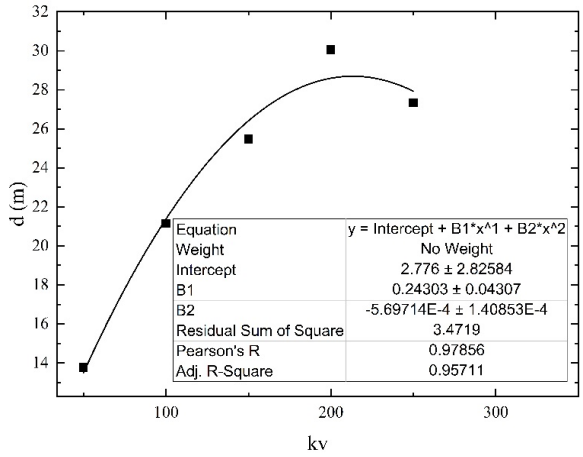

Figure 20. Fitting curve of the longest distance d that can be reached by oil spill at different k_v within 7 s.

According to the above fitting equation, with the increase in k_v, the maximum horizontal spreading distance of the oil spill does not always increase but reaches the maximum when k_v is 200. After that, with the increase in k_v, the horizontal spreading distance of the oil spill gradually decreases.

5.4. The Impact of the Same k_v on the Spread of Oil Spills

When k_v is constant, as shown in Figures 13 and 21, when the oil spill is at 0.05 s, with the increase in leakage speed and water flow speed, the entrainment vortex formed by the oil spill becomes larger and more obvious. In the case of leakage at 1 s, the vertical height of the oil spill gradually increases with the increase in both the leakage speed and the water flow speed. When k_v is the same, the ocean current speed and the oil spill speed increase proportionally, and the spilled oil migration pattern is equivalent to the migration pattern that just alters the ocean current speed. However, as the oil spill speed increased, the spill tilted to the right and washed away sooner. At 7 s, when k_v is the same, the height of the oil spill spreading with higher oil leakage speed and ocean current speed is smaller, but the distance of horizontal spreading to the right is longer.

The horizontal migration distance of oil spills under different working conditions is shown in Figure 22. Under the same k_v, the horizontal migration distance of an oil spill increases with the proportional increase in oil spill speed and ocean current speed. This is due to the fact that the initial speed of the oil spill and the speed of the ocean current are both high, and as the time of action on the oil spill rises, so does the horizontal spreading distance. When the oil spill speeds are 10 m/s, 30 m/s, and 50 m/s, respectively, under three working conditions and the ocean current speeds are 0.2 m/s, 0.6 m/s, and 1.0 m/s, respectively, the simulated data are fitted, and the adjustment coefficient R^2 is 0.942, 0.884, and 0.925, respectively. The fitting formula obtained is as follows:

$$y = 0.856x + 0.576 \quad (17)$$

$$y = 1.956x + 2.087 \quad (18)$$

$$y = 2.437x + 2.455 \quad (19)$$

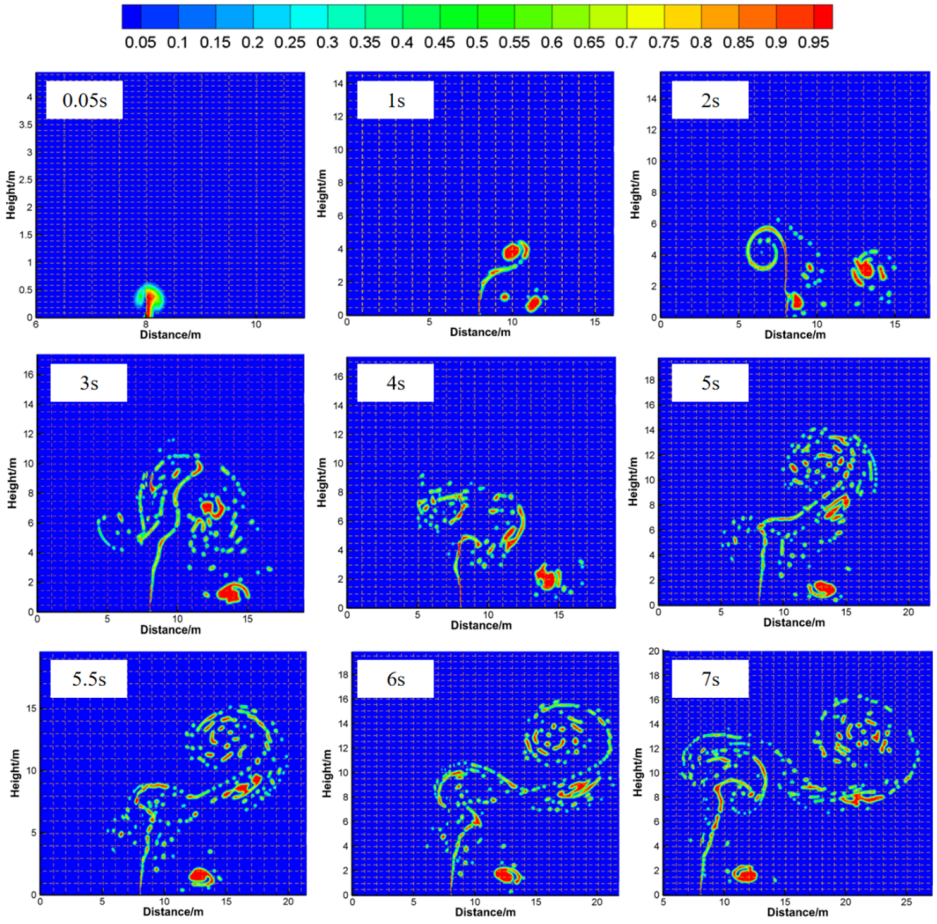

Figure 21. Ocean current speed of 1.0 m/s, leakage speed of 50 m/s, k_v = 50, oil spill spreading.

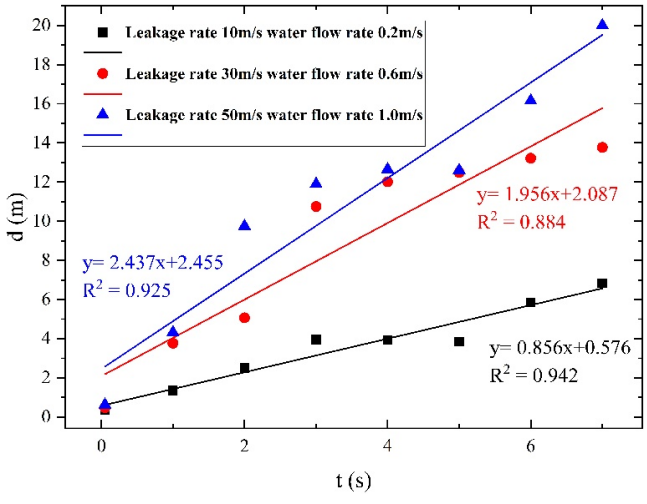

Figure 22. The horizontal drift distance of the oil spill at different times (d: Horizontal drift distance of oil spill).

According to the above fitting equation, it can be seen that the slope of the fitting curve of the horizontal spreading distance and time of the oil spill gradually increases when k_v is the same. The slope is the horizontal migration speed, which is 0.856 m/s, 1.956 m/s, and 2.437 m/s, respectively.

Figure 23 shows the vertical spreading distance of an oil spill under different working conditions. When k_v is the same, the vertical spreading distance of an oil spill increases

with the increase in oil spill speed and ocean current speed in the same proportion, showing the same law as the horizontal migration distance. When the oil spill speed is 40 m/s, 120 m/s, and 200 m/s, respectively, and the ocean current speed is 0.2 m/s, 0.6 m/s, and 1.0 m /s, respectively, the simulated data are fitted, and the adjustment coefficient R^2 is 0.909, 0.908, and 0.219, respectively. The fitting formula is as follows:

$$y = 2.328x + 3.898 \tag{20}$$

$$y = 3.671x + 5.647 \tag{21}$$

$$y = 3.792x + 9.507 \tag{22}$$

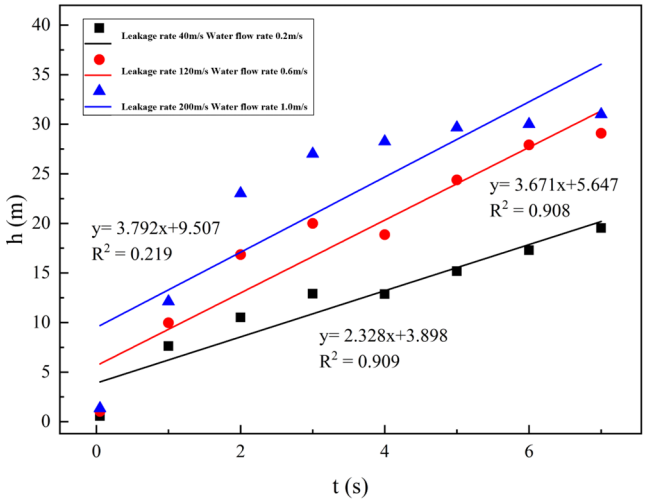

Figure 23. The vertical rising height trend of the oil spill at different times with k_v (h: Vertical spreading height of oil spill).

According to the above fitting equation, it can be seen that when k_v is the same, the slope of the fitting curve between the vertical spreading height of the oil spill and time gradually increases. The slope represents the vertical spreading speed, which is 2.328 m/s, 3.671 m/s, and 3.792 m/s, respectively.

Since the R^2 values of the above fitting are all less than 0.9, it indicates that the one-time fitting curve has a poor degree of fitting to the observed value. The fitting curve is modified to a cubic function to fit the observed value. The results are as follows:

Figure 24 shows the fitting curve of the oil spill rising height when k_v is the same. The adjustment coefficient R^2 is 0.991, 0.977, and 0.995, respectively. The fitting formula is as follows:

$$y = 0.545 + 7.905x - 1.692x^2 + 0.137x^3 \tag{23}$$

$$y = 0.828 + 10.965x - 2.045x^2 + 0.153x^3 \tag{24}$$

$$y = 0.106 + 16.139x - 2.982x^2 + 0.187x^3 \tag{25}$$

Figure 25 shows the fitting curve of the oil spill horizontal spreading distance when k_v is the same. The adjustment coefficient R^2 is 0.965, 0.971, and 0.984, respectively. The fitting formula is as follows:

$$y = 0.099 + 1.934x - 0.393x^2 + 0.036x^3 \tag{26}$$

$$y = 0.147 + 3.948x - 0.078x^2 + 0.022x^3 \quad (27)$$

$$y = 0.338 + 7.601x - 1.686x^2 + 0.145x^3 \quad (28)$$

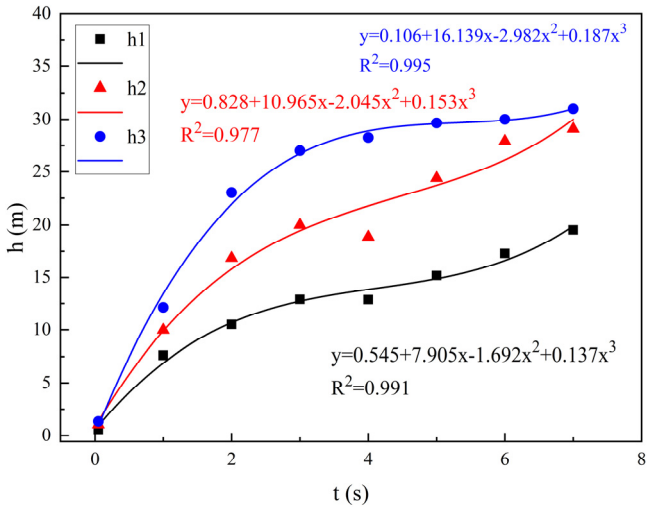

Figure 24. Cubic fitting curve of vertical rising height of oil spill under the same k_v (h: Vertical spreading height of oil spill; h1: Leakage rate 40 m/s water flow rate 0.2 m/s; h2: Leakage rate 120 m/s water flow rate 0.6 m/s; h3: Leakage rate 200 m/s water flow rate 1 m/s).

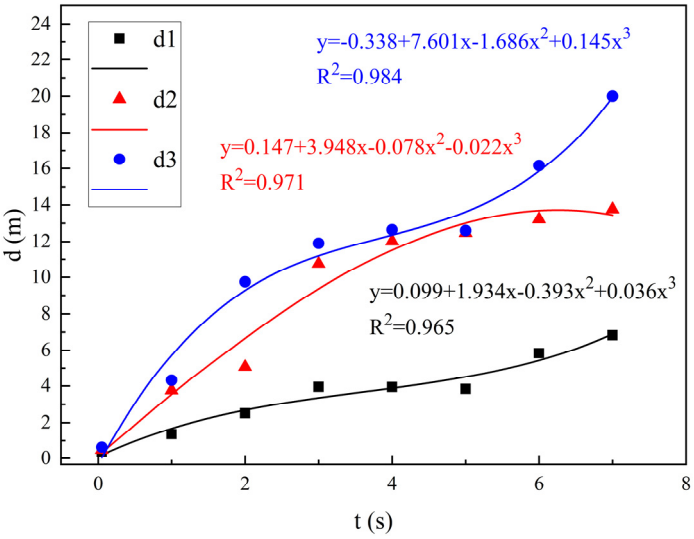

Figure 25. Cubic fitting curve of horizontal spreading distance of oil spill under the same k_v (d: Horizontal drift distance of oil spill; d1: Leakage rate 10 m/s water flow rate 0.2 m/s; d2: Leakage rate 30 m/s water flow rate 0.6 m/s; d3: Leakage rate 50 m/s water flow rate 1 m/s).

6. Conclusions

This article provides fitting curves for the actual oil spill migration velocity under different k_v values, which can be used to better understand the trend of oil spills. k_v is the ratio of leakage velocity to ocean current velocity. The oil spill spreading under different ocean current speeds, leakage speed, and the proportion of leakage speed to ocean current speed are studied. The analysis of the oil spill spreading law is performed last. The following findings have been reached based on the results of our numerical simulation and experiments:

(1) A numerical simulation was used to model the process of oil seeping from the oil spill hole. The simulation area was 30 m high, and the calculation time was 7 s. When the water flow rate is constant, the vertical spreading velocity of an oil spill increases as k_v increases. When the leakage rate is constant, the horizontal spreading distance climbs as k_v decreases. The greatest oil spill spreading height does, however, decrease as the water flow speed increases; the maximum oil spill spreading height at 0.2 m/s is 19.53 m.

(2) The maximum height of the oil spill can be 20.92 m for an oil spill with a speed of 50 m/s. As the speed of the leakage grows, so do the height and horizontal distance of the oil spill; the greater the speed of the oil spill, the higher the maximum height of the oil spill will be. With an increase in leakage speed, the slope of the line graph representing the height of the oil spill rises.

(3) When k_v is different, an oil spill's horizontal spreading distance and vertical spreading height grow as k_v rises. The vertical spreading speed of an oil spill rapidly reduces at the start of the spill when k_v = 50, 100, or 150. When the water flow rate is constant, the vertical spreading velocity of an oil spill increases as k_v increases. Under conditions of a constant leakage rate, the horizontal spreading distance increases as k_v decreases.

(4) In the process of underwater oil spill transport, the ratio of oil spill speed to ocean current speed, k_v, is fitted to the highest height that the oil spill can reach within a certain period of time, and the fitting curve is $y = 3.274 + 0.17x - 3.491x^2$; the maximum distance of horizontal migration of oil spill within a certain period of time, and the fitting curve is $y = 2.776 + 0.243x - 5.697x^2$.

(5) When k_v is the same, the leakage speed and flow speed increase simultaneously, but the migration pattern of an oil spill is similar to that of only a changing flow speed. At 7 s, when k_v is the same, the height of the oil spill spreading with higher oil leakage speed and ocean current speed is smaller, but the distance of horizontal spreading to the right is longer.

(6) K_v is a research indicator used to study diffusion patterns following oil spills. When an oil spill accident occurs on the sea surface, the movement trajectory and destination of the oil spill can be judged in advance, which can respond in time, and the oil pollution can be effectively cleaned up in the first place according to the emergency plan to control the spread of marine pollution. By simulating the diffusion law of the oil spill, some targeted measures can be taken to prevent the oil leakage accident on the submarine pipeline, which plays a very important role in environmental protection.

Author Contributions: Conceptualization, H.J.; methodology, H.J., Y.W. and T.W.; software, H.J. and Y.W.; validation, H.J., Y.W. and T.W.; formal analysis, H.J., Y.W. and T.W.; investigation, H.J., Y.W. and T.W.; resources, H.J., K.Y. and Z.X.; data curation, H.J. and Y.W.; writing—original draft preparation, H.J. and Y.W.; writing—review and editing, H.J. and T.W.; visualization, H.J. and Y.W.; supervision, H.J.; project administration, H.J.; funding acquisition, H.J. and K.Y. All authors have read and agreed to the published version of the manuscript.

Funding: This research was funded by the National Natural Science Foundation of China (No. 52204204, 51704041, 51574046, 21927815), the Joint Project of Industry-University-Research of Jiangsu Province (No. BY2021421), the Natural Science Foundation of Jiangsu Province (No. BK20150269), and the Major Research Plan of the Oil and Gas Storage and Transportation Laboratory of Jiangsu Province (SCZ1211200004/004).

Data Availability Statement: The datasets used and/or analyzed during the current study are available from the corresponding author upon reasonable request.

Conflicts of Interest: The authors declare that they have no known competing financial interest or personal relationships that could have appeared to influence the work reported in this paper.

References

1. Naz, S.; Iqbal, M.F.; Mahmood, I.; Allam, M. Marine oil spill detection using Synthetic Aperture Radar over Indian Ocean. *Mar. Pollut. Bull.* **2021**, *162*, 111921. [CrossRef]
2. Romero, I.C.; Toro-Farmer, G.; Diercks, A.R.; Schwing, P.; Muller-Karger, F.; Murawski, S.; Hollander, D.J. Large-scale deposition of weathered oil in the Gulf of Mexico following a deep-water oil spill. *Environ. Pollut.* **2017**, *228*, 179–189. [CrossRef]
3. Zhu, Z.; Zhang, B.; Cai, Q.; Ling, J.; Chen, B. Fish Waste Based Lipopeptide Production and the Potential Application as a Bio-Dispersant for Oil Spill Control. *Front. Bioeng. Biotechnol.* **2020**, *8*, 734. [CrossRef] [PubMed]
4. Li, Q.; Zhang, C.; Yang, Y.; Ansari, U.; Han, Y.; Li, X.; Cheng, Y. Preliminary experimental investigation on long-term fracture conductivity for evaluating the feasibility and efficiency of fracturing operation in offshore hydrate-bearing sediments. *Ocean Eng.* **2023**, *281*, 114949. [CrossRef]
5. Etkin, D.S.; Nedwed, T.J. Effectiveness of mechanical recovery for large offshore oil spills. *Mar. Pollut. Bull.* **2020**, *163*, 111848. [CrossRef]
6. Wang, C.; Bing, C.; Zhang, B.; He, S.; Zhao, M. Fingerprint and weathering characteristics of crude oils after Dalian oil spill, China. *Mar. Pollut. Bull.* **2013**, *71*, 64–68. [CrossRef]
7. Shi, Z.; Li, Y.; Dong, L.; Guan, Y.; Bao, M. Deep remediation of oil spill based on the dispersion and photocatalytic degradation of biosurfactant-modified TiO_2. *Chemosphere* **2021**, *281*, 130744. [CrossRef]
8. Li, Q.; Zhao, D.; Yin, J.; Zhou, X.; Li, Y.; Chi, P.; Han, Y.; Ansari, U.; Cheng, Y. Sediment Instability Caused by Gas Production from Hydrate-bearing Sediment in Northern South China Sea by Horizontal Wellbore: Evolution and Mechanism. *Nat. Resour. Res.* **2023**, *32*, 1595–1620. [CrossRef]
9. Barron, M.G.; Vivian, D.N.; Heintz, R.A.; Yim, U.H. Long-Term Ecological Impacts from Oil Spills: Comparison of Exxon Valdez, Hebei Spirit, and Deepwater Horizon. *Environ. Sci. Technol.* **2020**, *54*, 6456–6467. [CrossRef]
10. Yang, Z.; Chen, Z.; Lee, K.; Owens, E.; Taylor, E.J.M.P.B. Decision support tools for oil spill response (OSR-DSTs): Approaches, challenges, and future research perspectives. *Mar. Pollut. Bull.* **2021**, *167*, 112313. [CrossRef]
11. Mohammadiun, S.; Hu, G.; Gharahbagh, A.A.; Li, J.; Hewage, K.; Sadiq, R. Intelligent computational techniques in marine oil spill management: A critical review. *J. Hazard. Mater.* **2021**, *419*, 126425. [CrossRef]
12. Hammouda, S.B.; Chen, Z.; An, C.; Lee, K. Recent advances in developing cellulosic sorbent materials for oil spill cleanup: A state-of-the-art review. *J. Clean. Prod.* **2021**, *311*, 127630. [CrossRef]
13. Jianliang, X.; Nana, L.; Xinfeng, X.; Yu, B.; Yu, G.; Kunhua, W.; Xiangming, H.; Dongle, C.; Qing, J. Durable hydrophobic Enteromorpha design for controlling oil spills in marine environment prepared by organosilane modification for efficient oil-water separation. *J. Hazard. Mater.* **2022**, *421*, 126824. [CrossRef] [PubMed]
14. Feng, Q.; An, C.; Chen, Z.; Yin, J.; Zhang, B.; Lee, K.; Wang, Z. Investigation into the impact of aged microplastics on oil behavior in shoreline environments. *J. Hazard. Mater.* **2022**, *421*, 126711. [CrossRef] [PubMed]
15. He, G.; Liang, Y.; Li, Y.; Wu, M.; Sun, L.; Xie, C.; Li, F. A method for simulating the entire leaking process and calculating the liquid leakage volume of a damaged pressurized pipeline. *J. Hazard. Mater.* **2017**, *332*, 19–32. [CrossRef] [PubMed]
16. Burgherr, P. In-depth analysis of accidental oil spills from tankers in the context of global spill trends from all sources. *J. Hazard. Mater.* **2007**, *140*, 245–256. [CrossRef]
17. Zhu, H.; Lin, P.; Pan, Q. A CFD (computational fluid dynamic) simulation for oil leakage from damaged submarine pipeline. *Energy* **2014**, *64*, 887–899. [CrossRef]
18. Ji, H.; Guo, J.; Zhang, G.; Yang, K.; Jiang, J.; Wang, Y.; Xing, Z.; Bi, H. Multi-Factor Coupling Analysis of Porous Leakage in Underwater Gas Pipelines. *Processes* **2023**, *11*, 1259. [CrossRef]
19. Li, Q.; Han, Y.; Liu, X.; Ansari, U.; Cheng, Y.; Yan, C. Hydrate as a by-product in CO_2 leakage during the long-term sub-seabed sequestration and its role in preventing further leakage. *Environ. Sci. Pollut. Res.* **2022**, *29*, 77737–77754. [CrossRef]
20. Li, Q.; Wang, F.; Wang, Y.; Zhou, C.; Chen, J.; Forson, K.; Miao, R.; Su, Y.; Zhang, J. Effect of reservoir characteristics and chemicals on filtration property of water-based drilling fluid in unconventional reservoir and mechanism disclosure. *Environ. Sci. Pollut. Res.* **2023**, *30*, 55034–55043. [CrossRef]
21. Raznahan, M.; An, C.; Li, S.S.; Geng, X.; Boufadel, M. Multiphase CFD simulation of the nearshore spilled oil behaviors. *Environ. Pollut.* **2021**, *288*, 117730. [CrossRef] [PubMed]
22. Meng, H.; An, X. Dynamic risk analysis of emergency operations in deepwater blowout accidents. *Ocean Eng.* **2021**, *240*, 109928. [CrossRef]
23. Ainsworth, C.H.; Chassignet, E.P.; French-McCay, D.; Beegle-Krause, C.J.; Berenshtein, I.; Englehardt, J.; Fiddaman, T.; Huang, H.; Huettel, M.; Justic, D.; et al. Ten years of modeling the Deepwater Horizon oil spill. *Environ. Model. Softw.* **2021**, *142*, 105070. [CrossRef]
24. Chen, H.; An, W.; You, Y.; Lei, F.; Zhao, Y.; Li, J. Numerical study of underwater fate of oil spilled from deepwater blowout. *Ocean Eng.* **2015**, *110*, 227–243. [CrossRef]
25. Paiva, P.M.; Lugon Junior, J.; Barreto, A.N.; Silva, J.A.F.; Silva Neto, A.J. Comparing 3d and 2d computational modeling of an oil well blowout using MOHID platform—A case study in the Campos Basin. *Sci. Total Environ.* **2017**, *595*, 633–641. [CrossRef]
26. Berry, A.; Dabrowski, T.; Lyons, K. The oil spill model OILTRANS and its application to the Celtic Sea. *Mar. Pollut. Bull.* **2012**, *64*, 2489–2501. [CrossRef]

27. González, M.; Ferrer, L.; Uriarte, A.; Urtizberea, A.; Caballero, A. Operational Oceanography System applied to the Prestige oil-spillage event. *J. Mar. Syst.* **2008**, *72*, 178–188. [CrossRef]
28. Lamine, S.; Xiong, D. Guinean environmental impact potential risks assessment of oil spills simulation. *Ocean Eng.* **2013**, *66*, 44–57. [CrossRef]
29. Sun, Y.; Cao, X.; Liang, F. Investigation on underwater spreading characteristics and migration law of oil leakage from damaged submarine pipelines. *Process Saf. Environ. Prot.* **2019**, *127*, 330–347. [CrossRef]
30. Cao, X.; Wen, J.; SUN, Y. Numerical simulation on diffusion and drift laws of crude oil due to leakage of submarine pipeline. *J. Saf. Sci. Technol.* **2018**, *14*, 20–26.
31. Chen, J. *Numerical Simulation of Oil Spill Transport in Submarine Pipeline*; Dalian University of Technology: Dalian, China, 2015.
32. Daskiran, C.; Xue, X.; Cui, F.; Katz, J.; Boufadel, M.C. Impact of a jet orifice on the hydrodynamics and the oil droplet size distribution. *Int. J. Multiph. Flow* **2022**, *147*, 103921. [CrossRef]
33. Yapa, P.D.; Zheng, L.; Chen, F. A Model for Deepwater Oil/Gas Blowouts. *Mar. Pollut. Bull.* **2001**, *43*, 234–241. [CrossRef] [PubMed]
34. Chen, F.; Yapa, P.D. Modeling gas separation from a bent deepwater oil and gas jet/plume. *J. Mar. Syst.* **2004**, *45*, 189–203. [CrossRef]
35. Yapa, P.D. Calculation of oil droplet size distribution in ocean oil spills: A review. *Mar. Pollut. Bull.* **2018**, *135*, 723–734.
36. Brandvik, P.J.; Johansen, O.; Leirvik, F.; Farooq, U.; Daling, P.S. Droplet breakup in subsurface oil releases—Part 1: Experimental study of droplet breakup and effectiveness of dispersant injection. *Mar. Pollut. Bull.* **2013**, *73*, 319–326. [CrossRef] [PubMed]
37. Qi, J.; Li, J.; An, W. Underwater oil spill behavior and its fate in deep water area. *Ocean Dev. Manag.* **2013**. [CrossRef]
38. Xiao, J. *The Research on the Size and the Ascending Velocity of Oil Drops Spilling from Tiny Holes of Seabed Pipelines*; Dalian University of Technology: Dalian, China, 2007.
39. Zang, X. *Study on Characteristics of Pipeline Leakage and Oil-Gas Diffusion*; JiMei University: Xiamen, Fujian, 2013.
40. Yang, Y. The Transport-Diffusion Forecast of the Oil Spill from Seabed Pipeline and Its Application in the Beibu Gulf Ocean University of China. 2009. Available online: https://kns.cnki.net/kcms2/article/abstract?v=3uoqIhG8C475KOm_zrgu4lQARvep2SAk6at-NE8M3PgrTsq96O6n6a2HjcfrbPK42qC4k-lTdLB9L-Dt5-bbZzN-gaMIV3p6&uniplatform=NZKPT (accessed on 29 June 2023).
41. Gao, Q.; Zhu, Y.; Lin, J. Mathematical simulation of oil spill from seabed pipeline. *J. Dalian Marit. Univ.* **2007**, *33*, 169–171.
42. Ji, H.; Xu, M.; Huang, W.; Yang, K. The Influence of Oil leaking rate and Ocean Current Velocity on the Migration and Diffusion of Underwater Oil Spill. *Sci. Rep.* **2020**, *10*, 9226. [CrossRef]
43. Akhlaghi, M.; Mohammadi, V.; Nouri, N.M.; Taherkhani, M.; Karimi, M. Multi-Fluid VoF model assessment to simulate the horizontal air-water intermittent flow. *Chem. Eng. Res. Des.* **2019**, *152*, 48–59. [CrossRef]
44. Liu, R.; Ding, S.; Ju, G. Numerical Study of Leakage and Diffusion of Underwater Oil Spill by Using Volume-of-Fluid (VOF) Technique and Remediation Strategies for Clean-Up. *Processes* **2022**, *10*, 2338. [CrossRef]
45. Maele, K.V.; Merci, B. Application of two buoyancy-modified—Turbulence models to different types of buoyant plumes. *Fire Saf. J.* **2006**, *41*, 122–138. [CrossRef]
46. Lawal, M.S.; Fairweather, M.; Gogolek, P.; Ingham, D.B.; Ma, L.; Pourkashanian, M.; Williams, A. CFD predictions of wake-stabilised jet flames in a cross-flow. *Energy* **2013**, *53*, 259–269. [CrossRef]
47. Rohdin, P.; Moshfegh, B. Numerical predictions of indoor climate in large industrial premises. A comparison between different k–ε models supported by field measurements. *Build. Environ.* **2007**, *42*, 3872–3882. [CrossRef]
48. Ji, M.K.; Utomo, R.; Woo, R.; Lee, R.; Jeong, R.; Chung, R. CFD investigation on the flow structure inside thermo vapor compressor. *Energy* **2010**, *35*, 2694–2702. [CrossRef]
49. Hirt, C.W.; Nichols, B.D. Volume of fluid (VOF) method for the dynamics of free boundaries. *J. Comput. Phys.* **1981**, *39*, 201–225. [CrossRef]
50. Hieu, P.D.; Katsutoshi, T.; Ca, V.T. Numerical simulation of breaking waves using a two-phase flow model. *Appl. Math. Model.* **2004**, *28*, 983–1005. [CrossRef]
51. Li, X.; Han, Z.; Yang, S.; Chen, G. Underwater gas release modeling and verification analysis. *Process Saf. Environ. Prot.* **2020**, *137*, 8–14. [CrossRef]
52. Issakhov, A.; Zhandaulet, Y. Numerical study of dam break waves on movable beds for various forms of the obstacle by VOF method. *Ocean Eng.* **2020**, *209*, 107459. [CrossRef]
53. Seif, M.S.; Asnaghi, A.; Jahanbakhsh, E. Implementation of PISO algorithm for simulating unsteady cavitating flows. *Ocean Eng.* **2010**, *37*, 1321–1336. [CrossRef]